Lecture 2 ARRAY LAYOUT FOR SOURCE INVERSION
Subject 4 Strong Seismic Ground Motion Array Layout for Source Studies: Three Attempts

1. INTRODUCTION

Understanding of the nature of high-frequency strong seismic ground motion is a crucial problem in both seismology and earthquake engineering. Although local site effects on strong-motion records have been undoubtedly verified by numerous studies, almost no study has been done to investigate source effects that are closely related to damage and intensity patterns in the high-frequency range. The most likely reason is luck of well instrumented earthquakes available for detailed source studies. The best example to demonstrate such source effects might be Hartzell and Iida's study (1990), which perhaps used the best instrumented earthquake to date.

Source inversion is the most powerful tool to investigate source effects. However, large inconsistencies have been often seen among source inversion results. Such typical inconsistency was exemplified in the 1979 Imperial Valley earthquake (e.g. Olson and Apsel, 1982; Hartzell and Heaton, 1983; Archuleta, 1984). The inconsistencies seem to come mainly from the differences in the model construction and insufficient station distribution.

At the International Workshop on Strong-Motion Earthquake Instrumented Arrays held in Honolulu, Hawaii in 1978 (Iwan), a preferable array configuration was first proposed on the basis of empirical judgement. According to the source type, three different array networks for source mechanism and wave propagation studies were presented. Only few quantitative attempts have been made to estimate effects of station array. Spudich and Oppenheimer (1986) measured the resolving power of a hypothetical, differential seismograph array by performing frequency-wavenumber analysis and ray-tracing. Olson and Anderson (1988) showed that the assumed solution was not recovered by their frequency-domain inversion method, and that the goodness of recovery was dependent upon the station array, while Iida *et al.* (1988) represented effects of array configuration by a single parameter on the basis of their method (Miyatake *et al.*, 1986). Although these studies used too simple Green's functions, the significance of good strong-motion array was undoubtedly shown.

In our present study, we (1) obtain relationship between the accuracy of a source inversion and fault-array parameters, (2) present the optimum array geometry for the source inversion, and (3) investigate effects of existing array networks. Our conclusion is that we can reasonably design strong-motion array in a given condition.

2. METHODS

Since our method was explained in a previous study (Iida *et al.*, 1990b), we give here a very brief summary. We use the Wolberg's prediction analysis (Wolberg, 1967) to calculate the accuracy of a waveform inversion solution from errors contained in the data by using a principle of error propagation. We divide the entire fault into many subfaults to deal with a detailed history of rupturing and use the displacement waveform representation for each subfault. A complete Green's function in a semi-infinite elastic space is used. The seismic moment and the rupture onset time for each subfault are chosen as unknown parameters. They are determined using a least-squares criterion. We estimate the accuracy of the source inversion, σ by the maximum standard deviation of seismic moments for all subfaults, normalized by the seismic moment. Three sorts of simulations are done in the following.

---

* This lecture note is based on the paper of the same title written by Masahiro Iida, published on "Earthquake Engineering, Tenth World Conference, 1992 Balkema, Rotterdam. ISMB 90 5410 060 5".

3. RELATIONSHIP BETWEEN THE ACCURACY OF SOURCE INVERSION AND FAULT-ARRAY PARAMETERS (1ST SIMULATION)

A systematic analysis is done to obtain relationship between the accuracy of a source inversion and fault-array parameters (Iida *et al.*, 1990b). Strike-slip and dip-slip faults are assumed to be located at the center of a circular array (Fig. 1(a)). Several fault-array parameters are separately varied and their effects on the accuracy of the source inversion are evaluated.

Five fault parameters considered are (1) the number of subfaults, Ne; (2) the aspect ratio, Φ; (3) the dip angle, δ; (4) the fault depth, h; and (5) the rupture mode. We find that the normalized uncertainty, σ is roughly proportional to Ne^2, independent of fault mechanism (Fig. 1(b)). Depth resolution is worse than the resolution in the horizontal direction. The uncertainty does not depend much on the dip angle, the fault depth, and the rupture mode.

Array parameters are important because they can be controlled. Four parameters are examined: (1) the number of stations, Ns; (2) the array radius, R; (3) the azimuthal coverage of the source, ϕ; and (4) the components of the seismograms. The uncertainty, σ is found to roughly obey an inverse root dependence on Ns (Fig. 1(c)). Fig. 1(d) exhibits that the inversion uncertainty becomes minimum when the array radius, R is around 0.75 to 2.0 times the fault length. $\sigma \propto \phi^{-1}$ holds approximately in the case where Ns is kept proportional to ϕ, suggesting a remarkable contribution of the azimuthal coverage. The horizontal component parallel to the fault strike tends to contribute to a strike-slip fault, and the vertical component to a dip-slip fault. These simulations tell us that, while just an increase in the number of stations is not efficient, the azimuthal coverage of the source and the array size should be considered.

Furthermore, we attempt to demonstrate or refute the necessity of ocean bottom seismographs because no quantitative arguments on whether strong-motion ocean bottom seismographs are worth installing have yet been made (Iida *et al.*, 1990b). It is doubtful that our results are a strong incentive to deploy permanent ocean bottom stations in subduction zones.

4. OPTIMUM ARRAY GEOMETRY FOR SOURCE INVERSION (2ND SIMULATION)

We estimate the optimum array configuration for source inversion by trial and error for each of 3 typical faults, as shown in Fig. 2 (Iida, 1990). By 'optimum', we mean that the inversion solution becomes the most accurate with the same number of array stations and for the same process of fault rupturing. In some cases of the offshore fault simulation, validity of hypothetical strong-motion ocean bottom seismographs is again examined.

The optimum array configuration is presented in Fig. 2. The optimum array configurations are compared with the ones proposed at the Workshop (Iwan, 1978). The rightness of the empirical Workshop judgement is corroborated, and we are confident that the goodness of array configuration can be quantitatively measured by our method.

5. APPLICATION TO EXISTING STRONG-MOTION ARRAYS (3RD SIMULATION)

We evaluate the resolving power of four existing array networks (Iida *et al.*, 1990a). They are for the 1979 Imperial Valley and anticipated Parkfield, California earthquakes, and the 1968 Tokachi-oki and the anticipated Tokai, Japan earthquakes. In an attempt to evaluate the contribution of each station, we introduce two station parameters: 'time separation' and 'moment sensitivity'. The exact definition of the two parameters are given in another paper (Iida *et al.*, 1990a).

The results for the 1979 Imperial Valley earthquake are shown in the following. The surface fault trace

of this earthquake and the locations of strong-motion recording stations are displayed in Fig. 3(a). Undoubtedly, the spatial resolution predetermined by the subfault size is the dominant factor. When we increase the number of subfaults from 20 (the corresponding subfault area, Ae = 5x5 km^2) to 48 (Ae = 3x3 km^2) for the same number of stations, the inversion accuracy greatly drops from 0.88 to 5.46 (for the 13 stations of El Centro array of Fig. 3(a)), from 0.41 to 3.19 (for 20 stations distributed within the United States), and from 0.18 to 0.94 (for all 26 stations). We also find drastic change in the inversion uncertainty at each subfault due to the change in the number of stations, and a significant contribution of Mexican stations, which is probably due to a better azimuthal coverage (Fig. 3(b)). According to the two station parameters, the most useful stations appear to be located closely to the fault trace or on its southeastern extension (Fig. 3(a)).

The main results for other earthquakes are: (1) The array installed for the anticipated Parkfield earthquake seems to be satisfactory because of the intensive installation of many stations. (2) Detailed source inversion analysis cannot be expected in the 1968 Tokachi-oki, Japan earthquake because of both the large fault area and the offshore location. (3) An addition of several land stations on the west and north sides of the fault area is desirable to the present network for the anticipated Tokai, Japan earthquake.

6. STRONG-MOTION ARRAY DESIGN FOR SOURCE INVERSION

In this chapter, invoking results of physical wave simulations (Iida *et al.*, 1990b), basic guidelines and design policies of strong-motion array layout are provided.

The optimum station-array configuration heavily depends upon the physical (seismic) waves used for analysis (Iida *et al.*, 1990b). Because information obtained from distant surface waves or far-field body waves at distant stations cannot be recovered using any other waves, stations encircling the fault area with food azimuthal coverage are primarily required to unravel the source structure. These stations resolve the earlier stage of the rupturing process, while body waves in the source region resolve the later stage (Iida *et al.*, 1988).

Great dependence of the optimal array configuration on the fault mechanism is explainable. For a vertical strike-slip fault of strict phase requirements, stations immediately above the fault plane, which are robust at the vertical resolution, are needed. An inclined dip-slip fault favors a grid pattern of stations that appears to help many phases to be separated.

The simulations also present an important view concerning the choice in source inversion methods. Although a method of solving normal equations (e.g. Hartzell and Heaton, 1983) or an iterative least-square method (Kikuchi and Kanamori, 1982) may be general using stations which encircle the fault area, a differential array analysis using body-wave seismograms obtained from a source region (Spudich and Cranswick, 1984) is another powerful way available for source studies.

In conclusion, a current plausible policy of array design may be in the following If we consider intermediate frequency band (several seconds to several Hz), we should choose a method of solving normal equations or an iterative least-squares method using complete Green's functions. Then, the results from our studies are greatly available. First, according to the fault mechanism, a desirable array configuration is determined. Secondly, assuming the spatial resolution and the inversion accuracy required, the number of array stations is determined. When the target frequency range is very high (more than several Hz), a differential array analysis is recommended using only body waves. Exactly speaking, our techniques cannot be applied to this type of array since the analysis makes use of a difference in arrival times of distinguishable phases. Previously, our 1st (Iida *et al.*, 1986) and 2nd (Iida *et al.*, 1988) simulations were performed utilizing only far-field S waves. The results were considerably different from our present ones. They are able to make partial contribution to array layout design in that case.

7. REFERENCES

Archuleta, R.J (1984). A faulting model for the 1979 Imperial Valley earthquake, *J. Geophys. Res.*, **89**, 4559-4585.

Hartzell, S. and T. Heaton (1983). Inversion of strong ground motion and teleseismic waveform data for the fault rupture history of the 1979 Imperial Valley, California, earthquake, *Bull. Seismol. Soc. Am.*, **73**, 1553-1583.

Hartzell, S. and M. Iida (1990). Source complexity of the 1987 Whittier Narrows, California, earthquake from the inversion of strong motion records, *J. Geophys. Res.*, **95B**, 12475-12485.

Iida, M. (1990). Optimum strong-motion array geometry for source inversion -- II., *Earthquake Eng. Struct. Dyn.*, **19**, 35-44.

Iida, M., T. Miyatake and K. Shimazaki (1986). Relationship between the accuracy on source inversion and array parameters, and their interpretation, *Proc. 7th Japan Earthquake Eng. Symp.*, 451-456.

Iida, M., T. Miyatake and K. Shimazaki (1988). Optimum strong-motion array geometry for source inversion, *Earthquake Eng. Struct. Dyn.*, **16**, 1213-1225.

Iida, M., T. Miyatake and K. Shimazaki (1990a). Preliminary analysis of resolving power of existing strong-motion arrays for source inversion, *J. Phys. Earth*, **38**, 285-304.

Iida, M., T. Miyatake and K. Shimazaki (1990b). Relationship between strong-motion array parameters and the accuracy of source inversion, *Bull. Seismol. Soc. Am.*, **80**, 1533-1552.

Iwan, W.D. (Editor) (1978). Strong-motion earthquake instrument array. Proc. Int. Workshop Strong-Motion Earthquake Instrument Arrays, Honolulu, Hawaii.

Kikuchi, M. and H. Kanamori (1982). Inversion of complex body waves, *Bull. Seismol. Soc. Am.*, **72**, 491-506.

Miyatake, T., M. Iida and K. Shimazaki (1986). The effects of strong-motion array configuration on source inversion, *Bull. Seism. Soc. Am.*, **76**, 1173-1185.

Olson, A.H. and J.G. Anderson (1988). Implications of frequency-domain inversion of earthquake ground motions for resolving the space-time dependence of slip on an extended fault, *Geophysical Journal*, **94**, 443-455.

Olson, A H. and R. Apsel (1982). Finite faults and inverse theory with applications to the 1979 Imperial Valley earthquake, *Bull. Seismol. Soc. Am.*, **72**, 1969-2001.

Spudich, P. and E. Cranswick (1984). Direct observation of rupture propagation during the 1979 Imperial Valley earthquake using a short baseline accelerometer array, *Bull. Seismol. Soc. Am.*, **74**, 2083-2114.

Spudich, P. and D. Oppenheimer (1986). Dense seismograph array observations of earthquake rupture dynamics, in: *S. Das (Editor), Earthquake Source Mechanics, Geophys. Monograph*, **37**, 285-296.

Wolberg, J.R. (1967). Prediction analysis, Van Nostrand, Princeton, N.J.

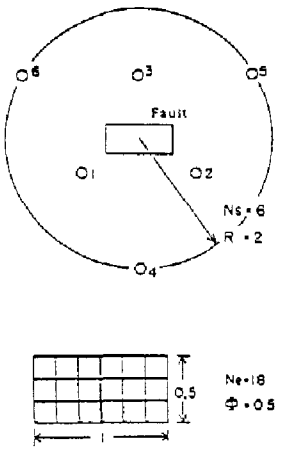

(a) fault-array layout used

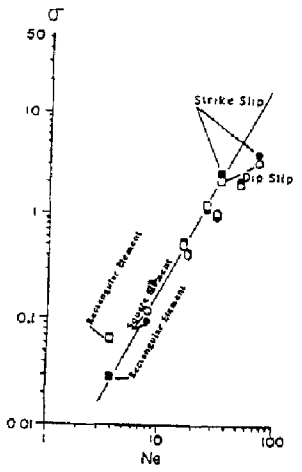

(b) σ vs. Ne

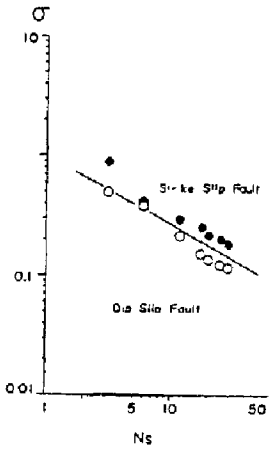

(c) σ vs. Ns

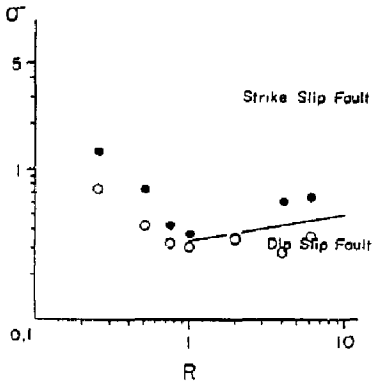

(d) σ vs. R

Fig. 1 Geometrical arrangement of faults and array stations and relationship between the accuracy of a source inversion, σ and fault-array parameters: (a) 2 kinds of faults located at the center of an array: a strike-slip fault with a dip angle, $\delta = 90°$ and a dip-slip fault with $\delta = 30°$. All distances are normalized by the fault length; (b) the inversion uncertainty, σ vs. the number of subfaults, Ne; (c) σ vs. the number of stations, Ns; (d) σ vs. the array radius, R.

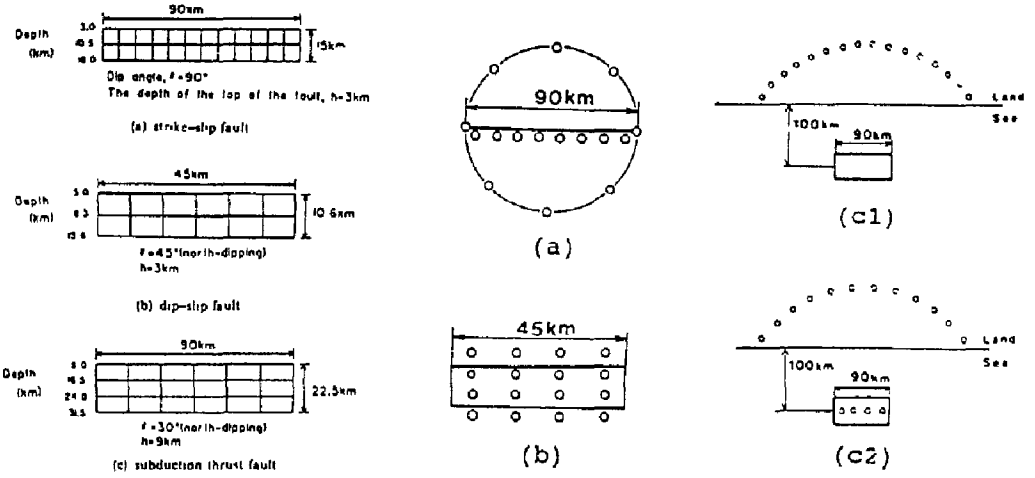

Fig. 2 Fault geometries used for investigating effects of array configurations on the source inversion (side views) and the optimum array configuration obtained for each of 3 fault geometries: (a) strike-slip; (b) dip-slip; and (c) subduction thrust fault (2 cases (c1) without and (c2) with strong-motion ocean bottom seismographs).

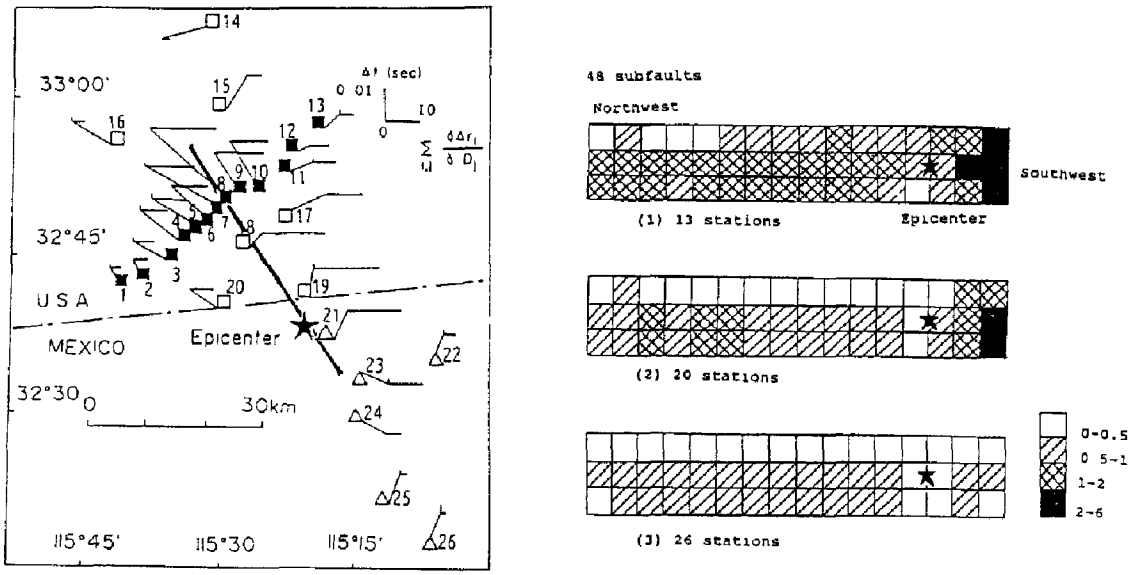

(a) Location map

(b) Inversion uncertainty

Fig. 3 Location map of the Imperial Valley section of the San Andreas fault showing strong-motion recording stations in (a), and the inversion uncertainty at all the subfaults in (b). 3 kinds of station arrays examined are 1) El Centro array perpendicularly crossing the fault trace (13 stations indicated by the solid squares), 2) 20 stations distributed within the United States (the solid and open circles), and 3) all 26 stations. Each inversion uncertainty at 48 subfaults determined for the 3 kinds of arrays (13, 20 and 26 stations) is indicated by ranking in (b). 'Time separation' and 'moment sensitivity' are evaluated at individual stations in the case of 48 subfaults in (a). The length of vertical bars show the time separation and that of horizontal bars shows the moment sensitivity.

Lecture 2 ARRAY LAYOUT FOR SOURCE INVERSION

Subject 5 Source Effects on Strong-Motion Records and Resolving Power of Strong-Motion Arrays for Source Inversion

1. INTRODUCTION

Understanding the nature of high-frequency, strong seismic ground motion is a crucial problem in both seismology and earthquake engineering. Although the local effects of strong-motion have been verified by numerous studies, almost no study has been made investigating source effects that are closely related to damage and intensity patterns in the high-frequency range. The most likely reason is a lack of well-instrumented earthquakes available for detailed source studies.

Source inversion is the most powerful tool for investigating source effects. However, large inconsistencies have been seen among source inversion results. A typical inconsistency was found in the results for the 1979 Imperial Valley earthquake (e.g., Olson and Apsel, 1982; Hartzell and Heaton, 1983; Archuleta, 1984). The differences in the results seem to come mainly from the differences in the model construction and insufficient station distribution for earthquake source studies. Inversion results should not be affected by the station distribution.

The deployment strategy of strong-motion seismographs has been only poorly explored. We have realized only empirically that source inversion results are strongly influenced by the number of stations and the array configuration. At the International Workshop on Strong-Motion Earthquake Instrumented Arrays held in Honolulu, Hawaii in 1978 (Iwan, 1978), a preferable array configuration was proposed on the basis of empirical judgement. That was the first proposal of an advantageous distribution of strong-motion array stations.

Three different array networks for source mechanism and wave propagation studies (depending on the source type), have been presented (Fig. 1). First, a comb-shaped array, comprising approximately 100-200 instruments, is recommended for a strike-slip source mechanism, as shown in Figure 1a. About half of the instruments are aligned at an average spacing of approximately 10 km along a line parallel to the fault strike on one side of the fault (because of the symmetry of the radiation patterns about the fault strike). The instruments contribute to the identification of the relative locations of constituent multiple events during a fault rupture process. The remaining instruments are arranged along a few legs extending perpendicular to the fault strike. These legs (which have a length of 40-100 km) extend linearly and are primarily available for the study of path effects. They also help in aiding in the discrimination of the multiple events.

Secondly, a two-dimensional array configuration, comprising approximately 100 instruments with a spacing of 2-10 km, is recommended for a dip-slip source mechanism (Fig. 1b). The instrument placement is intended to discover if the acceleration on the hanging wall is significantly different from that on the foot wall, and if there is significantly higher acceleration along the direction of strike or along the direction of propagation of the fault rupture. Thirdly, a linear or two-dimensional, narrow-band array, consisting of approximately 50-150 instruments, with an average spacing of 20 km, is recommended for a subduction thrust source mechanism (Fig. 1c). The instrument spacing is determined by the fault depth of the damaging shallow event. However, to date, no quantitative analysis has yet been carried out on how the array stations should be deployed, and which types of seismic waves should be analyzed.

Only few attempts have been made to estimate effects of station array. Spudich and Oppenheimer (1986) measured the resolving power of a hypothetical, differential seismograph array for high-frequency ground motions (> 1 Hz) by performing frequency-wavenumber analysis and ray tracing. Olson and Anderson (1988) showed that the assumed solution was not recovered by their frequency-domain inversion method with a minimum norm to obtain a unique solution, and that the quality of recovery was dependent upon the station array. Iida *et al.* (1988) represented the effects of array configuration by a single parameter on the basis of their method (Miyatake *et al.*, 1986). Although these studies used Green's functions that were too simple, the significance of good strong-motion

array was undoubtedly demonstrated.

I am developing two sorts of studies using a more realistic Green's function in order to indicate station-array effects. One is to evaluate the influence of array parameters, such as the number of stations and the azimuthal coverage of the array, and the other is to evaluate the influence of array configuration, which is difficult to parameterize. These studies are also applied to existing arrays. Since the quality of a station array should be associated with seismic waves to be analyzed, the relative significance of various seismic waves in the source inversion is examined. Although some of these studies have been recently published separately, the joint interpretation is very important in order to gain a general insight into the effectiveness of strong-motion arrays.

In this article we first summarize a study in which source effects on strong-motion records were demonstrated, for one of the best instrumented earthquakes to date, using a source inversion method. Secondly, three kinds of simulations are described in order to indicate the vulnerability of the resolving power of strong-motion arrays for a source inversion Finally, a joint interpretation of these studies is made and it is shown that we can reasonably design a strong-motion array for source inversion under a given condition.

2. SOURCE EFFECTS ON STRONG MOTION RECORDS

Here one example is given which demonstrates the source effects on strong-motion records using one of the best instrumented earthquake to date (Hartzell and Iida, 1990). Seventeen near-source, strong-motion records for the 1987 Whittier Narrows, California, earthquake, with a local magnitude of 5.9, are inverted to obtain the history of slip. The good station pattern, which forms a 360° azimuthal coverage of the source, is expected to give good resolution (Iida *et al.*, 1988; Iida, 1990) (Fig. 2). Band-pass filtered velocity records from 0.2 to 3.0 Hz are used. This frequency range is important in earthquake engineering and is responsible for much of an earthquake's damage and intensity

Figure 3 shows the contours of slip (in centimeters) for three inversion models. The similarity of the slip distribution in different rupture modes should be noted. The results show a complex rupture process within a small source volume. There is a good fit between the synthetic and recorded waveforms in both shape and amplitude, especially in the earlier parts of the records including the large-amplitude sections. This suggests that the inversion was very successful (Fig. 4). The ground motion in the epicentral region is predicted based upon the inferred distribution of slip from our inversion. The results are shown on the same scale in Figure 2, where peak velocities are contoured. This result is helpful in providing a good interpretation of the unusual intensity and damage patterns of this earthquake (Leyendecker *et al.*, 1988). We conclude that the ground motion can be explained by considering the source effects, coupled with the same averaged propagation path effects to each strong-motion station.

3. RESOLVING POWER OF STRONG-MOTION ARRAYS FOR SOURCE INVERSION

Above we confirmed that strong-motion seismograms were heavily controlled by source effects Another fact is that the differences in the model construction did not produce remarkable differences in the results. This means that the inconsistencies recognized among source inversion results are primarily due to the insufficient resolving power of strong-motion arrays After reviewing our method the dependence of the accuracy (the uncertainty) of an inversion solution on the array geometry is investigated and the contribution of various seismic waves to the accuracy of the inversion solution is measured

3.1 Methods

Since the method has been explained elsewhere (e.g., Iida *et al.*, 1990b), only a brief summary is given here. Wolberg's (1967) prediction analysis was used to calculate the accuracy of a waveform solution from errors contained in data by using a principle of error propagation. Most of the current source inversion studies deal with a detailed history of rupturing on a fault. We divided the entire fault into many subfaults and used a displacement

waveform representation for each subfault. A complete Green's function in a semi-infinite elastic space was used. A common, simple source-time function was assumed for each subfault. The seismic moment and the rupture onset time for each subfault were chosen as unknown parameters. The unknown parameters were determined using a least-squares criterion. Uncertainties were assumed for several known variables. We estimated the accuracy of the source inversion, σ, from the maximum standard deviation of the seismic moments for all subfaults, normalized by the seismic moment.

The theoretical waveform is a function of known and unknown parameters. The known parameters, whose uncertainties are taken into account (the dip angle, the strike direction, the slip angle, the wave amplitude and the arrival time) are denoted by x_p ($p = 1,\ldots, N_p$). The unknown parameters, the seismic moment and rupture onset time for each subfault are denoted by a_i ($i = 1,\ldots, N_a$). The wave amplitude for the jth time point at the kth station is expressed as $u^k(t_j) = f_j^k(x_{1kj},\ldots, x_{Npkj}; a_1,\ldots, a_{Nu})$. Two residuals, Ru_{kj} and Rx_{pkj} are defined as the differences between the observed and calculated values:

$$Ru_{kj} = U^k(t_j) - u^k(t_j) \qquad (1)$$

$$Rx_{pkj} = X_{pkj} - x_{pkj} \qquad (2)$$

where $U^k(t_j)$ and X_{pkj} ($p = 1,\ldots, N_p$) are the observed wave amplitude and the true value for the known parameter, respectively

The least-squares method is used to determine the values of the unknown parameters, a_i ($i = 1,\ldots, N_a$), which minimize the weighted sum of the squares of the residuals, S:

$$S = \sum_k \sum_j \left(Wu_{kj} Ru_{kj}^2 + \sum_p^{N_p} Wx_{pkj} Rx_{pkj}^2 \right) \qquad (3)$$

where $Wu_{kj} = 1/\sigma u_{kj}^2$ and $Wx_{pkj} = 1/\sigma x_{pkj}^2$; σu_{kj} = the standard deviation of the wave amplitude; and σx_{pkj} = the standard deviation of the known parameter

In general, the solution for the least-squares problem is obtained by solving normal equations in a matrix form. Following Wolberg's (1967) prediction analysis, however, the uncertainty of the ith unknown parameter, σa_i can be estimated by calculating the inverse of a matrix. In this case it is unnecessary to solve the actual normal equations. Three sorts of simulations are shown below.

3.2 Relationship between the accuracy of source inversion and fault-array parameters (1st simulation)

A systematic analysis was carried out to obtain a relationship between the accuracy of the source inversion and fault-array parameters (Iida *et al.*, 1990b). Strike-slip and dip-slip faults were assumed to be located at the center of a circular array (Fig. 5). Several fault-array parameters were separately varied and their effects on the accuracy of the source inversion were evaluated.

3.3 Fault parameters

Five parameters were considered: (1) the number of subfaults, N_e; (2) the aspect ratio, Φ; (3) the dip angle, δ; (4) the fault depth, h, and (5) the rupture mode. We found that the normalized uncertainty, σ, was roughly proportional to N_e^2, independent of the fault mechanism. Depth resolution was worse than the resolution in the horizontal direction. The uncertainty did not depend much on the dip angle, the fault depth and the rupture mode.

3.4 Array parameters

Array parameters are important because they can be controlled. Four parameters were examined: (1) the number

of stations, N_s; (2) the array radius, R; (3) the azimuthal coverage of the source, ϕ; and (4) the components of the seismograms. The effects of the array parameters are summarized in Figure 6.

The uncertainty, σ, is found to obey roughly an inverse root dependence on N_s (Fig. 6a). Together with the number of subfaults, N_e, the relationship, $\sigma \propto N_e^2/N_s^{1/2}$, suggests that numerous stations are required to analyze the detailed rupturing process. Figure 6b shows that the inversion uncertainty reaches a minimum when the array radius, R, is around 0.75-2.0 times the fault length. $\sigma \propto \phi^{-1}$ holds approximately in the case where N_s is kept proportional to ϕ (Fig. 6c). Note that $\sigma \propto N_s^{-1/2}$ holds when the azimuthal coverage is unchanged. Thus, the relationship $\sigma \propto \phi^{-1}$ under the condition of $\sigma \propto N_s$ implies a remarkable contribution from the azimuthal coverage. In Figure 6c, the relationship is determined by the case where the rupture direction is considered disadvantageous for the station array (i.e., the rupture propagates towards the station array, case A). Figure 6d shows that the horizontal component parallel to the fault strike tends to contribute to a strike-slip fault and the vertical component to a dip-slip fault.

3.5 Subduction thrust simulation

By conducting a test on the relative value of ocean bottom seismographs and surface seismographs for studying the rupture of a subduction event, we attempted to demonstrate or refute their necessity. Up to now, no quantitative arguments on whether strong-motion ocean bottom seismographs are worth installing have been made. At present, a semi-permanent, strong-motion ocean bottom seismograph does not exist, although temporary networks of strong-motion ocean bottom seismograph systems are being developed. Since 1978, relatively low cost seismic stations for measuring strong ground motion on the ocean bottom have been tested (Steinmetz *et al.*, 1979; 1981) These experiments indicate that an ocean bottom station is capable of recording ground accelerations up to about 1.0 g in the 0.1-10 Hz frequency band, with good reliability in most cohesive type soil conditions.

For this simulation, the fault and array geometry shown in Figure 7 was used. The numbers of surface stations and ocean bottom stations, N_s and N_o were varied separately to estimate their influence. The positions of the surface stations were fixed, as illustrated in Figure 7. Several patterns of ocean bottom stations were tested for each pair of N_s and N_o. They were intended to determine the best position for a combination of stations.

The effects of the increasing numbers of surface stations and ocean bottom stations on the inversion uncertainty are shown in Figure 8 Interestingly, the inversion uncertainty does not appear to saturate as the number of surface stations is increased in the absence of ocean bottom stations. The graph suggests that the effects of ocean bottom stations are not very dramatic. For example, even if we increase the number from 1 to 2 or from 2 to 4, a large drop in the inversion uncertainty is not seen. In order to recover the accuracy of the source inversion equivalent to that attained by using 4 ocean bottom stations (together with 4 surface stations), we have only to install 14 additional surface stations. In this case, 1 ocean bottom station is worth about 4 surface stations. It is doubtful whether our results are a strong incentive to deploy permanent ocean bottom stations in subduction zones.

This simulation also gives an interesting view concerning positions of ocean bottom stations. If we have only one instrument, it should be located on the opposite side to the land about the fault, not within the fault zone above the fault. In the case of two instruments, one should be deployed on the opposite side to the land while the other is within the fault zone. This indicates that azimuthal coverage is more important than proximity to the fault.

3.6 Optimum array geometry for strong-motion source inversion (2nd simulation)

By fixing the number of array stations at 16, we estimated the optimum array configuration by trial and error for each of three typical faults, as shown in Figure 9 (Iida, 1990). By "optimum" we mean that the inversion solution becomes the most accurate with the same number of array stations and for the same process of fault rupturing. A wide variety of array configurations was tested for the various faults. In some cases of offshore fault simulation, the usefulness of hypothetical strong-motion ocean bottom seismographs was examined.

The optimum array configuration for each fault geometry is presented in Figure 9. The optimum array configurations are compared with ones proposed at the International Workshop on Strong-Motion Earthquake Instrumented Array (Iwan, 1978). The desirable array configuration for a strike-slip fault appears to bear a little

resemblance to the comb-shaped one recommended at the Workshop (Fig. 1a). We should note the desirable array for a dip-slip fault (a grid pattern) is the same as the one suggested at the Workshop (Fig. 1b). For an offshore subduction thrust fault, the desirable configuration is similar to the Workshop proposal (Fig. 1c). The distribution of the estimation errors is uniform over the fault surface for the optimum array configuration.

3.7 Application to existing strong-motion arrays

As an actual application of our studies, we evaluated the resolving power of four existing array networks, while changing the spatial resolutions (subfault sizes) and arrays. Although this study has already been published (Iida *et al.*, 1990a), I here summarize the results to show the applicability of our studies.

The main results were.

(1) The array used for an analysis of the 1979 Imperial Valley earthquake is not suitable for source inversion.

(2) The array installed for the anticipated Parkfield earthquake by the end of 1985 seems to be satisfactory because of the intensive installation of many stations. The resolving power of the whole array would be increased by adding a few stations in the northwestern part of the fault or in distant areas for a better azimuthal coverage to the northwest of the fault.

(3) Detailed source inversion analysis cannot be expected for the 1968 Tokachi-oki, Japan, earthquake because of both the large fault area and lack of offshore stations.

(4) An addition of several land stations on the west and north sides of the fault area is desirable to the present network for the anticipated Tokai, Japan, earthquake. The resolving power of the whole array for this earthquake is strongly dependent upon a rupturing direction because station coverage of the southern oceanic part of the fault tends to be poor.

3.8 Physical waves on strong-motion source inversion (3rd simulation)

Which seismic waves contribute more to strong-motion source inversion? A correct answer to this question would shed light on the current strong-motion source inversions and array designs. It would also be helpful or estimating strong ground motions. A general argument on the relative significance of various physical waves for source inversion has not been made We attempt to give an answer by measuring the deterioration in the accuracy of the source inversion when various wave types are removed from the problem.

There seem to be two major differences between the real structure of the Earth and the homogeneous half-space used in our study: (1) the half-space has no Love waves; and (2) the half-space model may not be a good one in terms of the body waves that leave the source in a downwards direction and are observed at distant stations. If we can understand the physical processes that produce our results, we may be able to solve these problems. It would be very helpful to show which physical waves contribute more to the accuracy of the source inversion in the half-space model. It should be noted that, whereas an increase in the information about the source contained in the waveform decreases the uncertainty of the solution, it simultaneously complicates the waveform by interference with different phases and results in an increase in the uncertainty.

3.9 Dip angle and fault depth

Two factors on physical waves which may be worth examining are dip angle and fault depth. Dip angle is related to the relative separation in arrival times between seismic waves radiated from subfaults, while a shallow fault depth causes a preponderance of surface waves. The fault-array layout used (which is very similar to that in Figure 5), is shown in figure 10. Three stations are installed near the fault in order to emphasize the near-field terms. The three types of fault geometries used are summarized in Table 1. We can derive the effects of phase interference due to the relative separation in arrival times between seismic waves, using:

where t_n and t_s are the arrival times of the latest Rayleigh wave and the earliest S wave observed at the ith station. The calculated values are listed in Table 1. The average depth of faults is normalized by the fault length. A small PI means large phase interference due to fault geometry (i.e., dip angle). The first fault plane, with a 90° dip, will produce more severe phase interference than the other two planes. In addition, we will demonstrate the effects of surface wave dominance due to different source depths, using the second and third fault planes. The types of physical waves used at each station are shown in Figure 11. The same ten cases were tested for each of the three fault planes. Important comparisons are those of cases (1) and (3) for surface waves, cases (2) and (5) for near-field terms, and cases (4) and (10) for far-field terms.

TABLE 1

Three types of fault geometries used to study effects of various physical waves

Type	Slip direction	Dip angle (°)	Average depth of fault	PI
[1]	Strike-slip	90	0.35	1.02
[2]	Dip-slip	30	0.225	1.17
[3]	Dip-slip	30	0.35	1.13

Average depth of fault is normalized by fault length. Parameter, PI is introduced to measure phase interference due to fault geometry. See text for definition.

The accuracy of the source inversion is summarized in Figure 11. At first glance, we find that results for the fault planes of [2] and [3] show a different trend from a result for the fault plane of [1]. In the inclined dip-slip fault planes, primarily surface waves at distant stations contribute to the source inversion. Secondly, far-field terms are a main contributor in the absence of surface waves at distant stations, whereas near-field terms are not. Use of the shallower fault, [2], identical in geometry to the deeper fault, [3], shows that a predominance of surface waves reduces the uncertainty. On the other hand, no improvement can be made with respect to surface waves in the case of the vertical strike-slip fault plane of [1]. This is primarily due to phase interference. It should be noted that case 7, where only far-field waves are used, gives the best result. We can see that the far-field terms at both near-source and distant stations control the inversion uncertainty more strongly than the near-field terms.

3.10 Array radius

To investigate a relationship between the accuracy of the source inversion and the array radius for different physical waves, we conducted another simulation that used the fault-array layout shown in Figure 5. We used the same physical waves as the previous simulation. The fault plane of [2] was selected because it causes less phase interference and surface waves dominate. The results are plotted in Figure 12. Despite the fact that σ for a complete half-space solution degrades as R decreases, σ, for body waves, greatly improved in the ranges with small R.

4. DISCUSSION

Using these results we can discuss the adequacy of our half-space approximation. Whilst it is certain that Love waves would give further information at distant stations; since Love wave velocity is closer than Rayleigh wave velocity to S wave velocity, the phase interference between Love and S waves would be more severe. This leads to speculation that the accuracy of the source inversion would not be greatly improved by Love waves. In addition, body waves that leave the source downwards and are observed at distant stations appear to be contaminated with surface waves since they have large travel times. That is, the effects of such waves at distant stations are not drastic. In conclusion, the half-space approximation is basically adequate.

4.1 Strong-motion array design for source inversion

One important conclusion derived from our physical wave simulation is that the homogeneous half-space approximation gives realistic results. Therefore, basic guidelines on strong-motion array deployment for source studies can be provided and general comments can be given on the relationship between frequency band, inversion method, fault mechanism and array layout.

Our 1st and 2nd simulations are complimentary because the former systematic analysis describes the effects of array parameters while the latter simulation of the optimum array geometry exhibits effects which cannot be represented by the array parameters. Our 1st simulation is the first systematic attempt to evaluate numerically the resolving power of station array, although the absolute value is not very reliable. The result, $\sigma \propto 1/N_s^{1/2}$, suggests that an increase in the number of stations, alone, is not efficient for investigating the detailed fault rupturing process. Instead, array stations should be installed after taking into account the azimuthal coverage of the source and the array size.

Potentially more important are results derived from a simulation of an offshore subduction thrust. Our results do not appear to show convincingly that permanent ocean bottom stations are needed in subduction zones Since the present Green's function is still imperfect, we cannot give a detailed array configuration. Nevertheless, the consistency of our preferred array configurations with those proposed at the International Workshop on Strong-Motion Earthquake Instrumented Arrays (Iwan, 1978) is very significant. The correctness of the interpretation based upon empirical judgement is corroborated and we are confident that the merit of the array configuration can be quantitatively measured by our method.

The physical wave is a new concept that is essentially related to array layout for source studies. Plainly speaking, since the optimum station-array configuration depends heavily upon the seismic waves used for analysis, it should be interpreted in terms of physical waves. Since information obtained from distant surface waves or far-field body waves at distant stations, which is dependent upon the fault mechanism, cannot be recovered using any other waves, stations encircling the fault area with good azimuthal coverage are primarily required to unravel the source structure. These stations resolve the earlier stage of the rupturing process, while body waves in the source region resolve the later stage (Iida *et al.*, 1988). The large dependence of the optimal array configuration on the fault mechanism can also be explained. For a vertical strike-slip fault producing close phases, stations immediately above the fault plane, which are robust at the vertical resolution, are needed. An inclined dip-slip fault favors a grid pattern of stations that appears to aid the separation of many phases.

The relationship between the accuracy of the source inversion and the array radius for different physical waves is important for the choice of source inversion method. Figure 12 implies that a method of solving normal equations (e.g., Olson and Apsel, 1982; Hartzell and Heaton, 1983) or an iterative least-square method (Kanamori and Stewart, 1978; Kikuchi and Kanamori, 1982) may be rather general when using stations which encircle the fault area; a differential array analysis, however, using body-wave seismograms obtained form a source region (Spudich and Cranswick, 1984; Spudich and Oppenheimer, 1986), is another powerful way available for source studies.

One insufficient aspect in our series of studies is the lack of frequency-dependency consideration. In principle, this subject is not so difficult to examine. I have a plan for a combined study of actual source inversion and array layout evaluation, so as to verify practical usefulness of our methods. A current plausible policy for array design may be the following. If we consider the usual frequency band (several seconds to several Hz), we may choose a method of solving normal equations or an iterative least-squares method using complete Green's functions. Then, the results of our studies are adequate. First, according to the fault mechanism, a desirable array configuration can be determined. Secondly, assuming the spatial resolution (the size of subfaults) and the inversion accuracy required, the number of array stations can be determined using our formulations. When the target frequency range is very high ($>$ 10 Hz) a differential array analysis, using only body waves, is recommended. To be exact, our techniques cannot be applied to this type of array since the analysis makes use of a difference in the arrival times of distinguishable phases. Previously, our 1st (Iida *et al.*, 1986) and 2nd (Iida *et al.*, 1988) simulations were performed using only far-field S waves. The results were considerably different from the present ones. These results would be able to make a contribution to array layout design.

5. REFERENCES

Archuleta, R.J. (1984). A faulting model for the 1979 Imperial Valley earthquake, *J. Geophys. Res.*, **89**, 4559-4585.

Hartzell, S. and T. Heaton (1983). Inversion of strong ground motion and teleseismic waveform data for the fault rupture history of the 1979 Imperial Valley, California, earthquake, *Bull. Seismol. Soc. Am.*, **73**, 1553-1583.

Hartzell, S. and M. Iida (1990). Source complexity of the 1987 Whittier Narrows, California, earthquake from the inversion of strong motion records, *J. Geophys. Res.*, **95 (B)**, 12475-12485.

Iida, M. (1990). Optimum strong-motion array geometry for source inversion - II, *Earthquake Eng. Struct. Dyn.*, **19**, 35-44.

Iida, M., T. Miyatake and K. Shimazaki (1986). Relationship between the accuracy on source inversion and array parameters, and their interpretation, *Proc. 7th Japan Earthquake Eng. Symp.*, Earthquake Eng. Res. Liason Comm., Sci. Council of Japan, 451-456.

Iida, M., T. Miyatake and K. Shimazaki (1988). Optimum strong-motion array geometry for source inversion, *Earthquake Eng. Struct. Dyn.*, **16**, 1213-1225.

Iida, M., T. Miyatake and K. Shimazaki (1990a). Preliminary analysis of resolving power of existing strong-motion arrays for source inversion, *J. Phys. Earth*, **38**, 285-304.

Iida, M., T. Miyatake and K. Shimazaki (1990b). Relationship between strong-motion array parameters and the accuracy of source inversion, *Bull. Seismol. Soc. Am.*, **80**, 1533-1552.

Iwan, W.D. (Editor) (1978). Strong-motion earthquake instrument array, *Proc. Int. Workshop Strong-Motion Earthquake Instrument Arrays* (Honolulu, Hawaii) Int. Assoc. Earthquake Eng.

Kanamori, H. and G.S. Stewart (1978). Seismological aspects of the Guatemala earthquake of February 4, 1976, *J. Geophys. Res.*, **83 (B)**, 3427-3434.

Kikuchi, M. and H. Kanamori (1982). Inversion of complex body waves, *Bull. Seismol. Soc. Am.*, **72**, 491-506.

Leyendecker, E.V., L.M. Highland, M. Hopper, E.P. Arnold, P. Thenhaus and P. Powers (1988). The Whittier Narrows, California earthquake of October 1, 1987 -- Early results of isoseismal studies and damage surveys, *Earthquake Spectra*, **4**, 1-10.

Miyatake, T., M. Iida and K. Shimazaki (1986). The effects of strong-motion array configuration on source inversion, *Bull. Seismol. Soc. Am.*, **76**, 1173-1185.

Olson, A.H. and J.G. Anderson (1988). Implications of frequency-domain inversion of earthquake ground motions for resolving the space-time dependence of slip on an extended fault, *Geophys. J.*, **94**, 443-455.

Olson, A.H. and R. Apsel (1982). Finite faults and inverse theory with applications to the 1979 Imperial Valley earthquake, *Bull. Seismol. Soc. Am.*, **72**, 1969-2001.

Spudich, P. and E. Cranswick (1984). Direct observation of rupture propagation during the 1979 Imperial Valley earthquake using a short baseline accelerometer array, *Bull. Seismol. Soc. Am.*, **74**, 2083-2114.

Spudich, P. and D. Oppenheimer (1986). Dense seismograph array observations of earthquake rupture dynamics, In: S. Das, J. Boatwright and C.H. Scholz (Editors), *Earthquake Source Mechanics. Geophys. Monogr. Am. Geophys. Union*, **37**, 285-296.

Steinmetz, R.L., P.L. Donoho, J.D. Murff and G.V. Latham (1979). Soil coupling of a strong motion, ocean bottom seismometer, *11th Offshore Technology Conf. Proc.*, **4**, 2235-2249.

Steinmetz, R.L., J.D. Murff, G. Latham, A. Roberts, P. Donoho, L. Babb and T. Eichel (1981). Seismic instrumentation of the Kodiak shelf, *Mar. Geotechnol.*, **4**, 192-221.

Wolberg, J.R. (1967). Prediction analysis, Van Nostrand, Princeton, N J., 291.

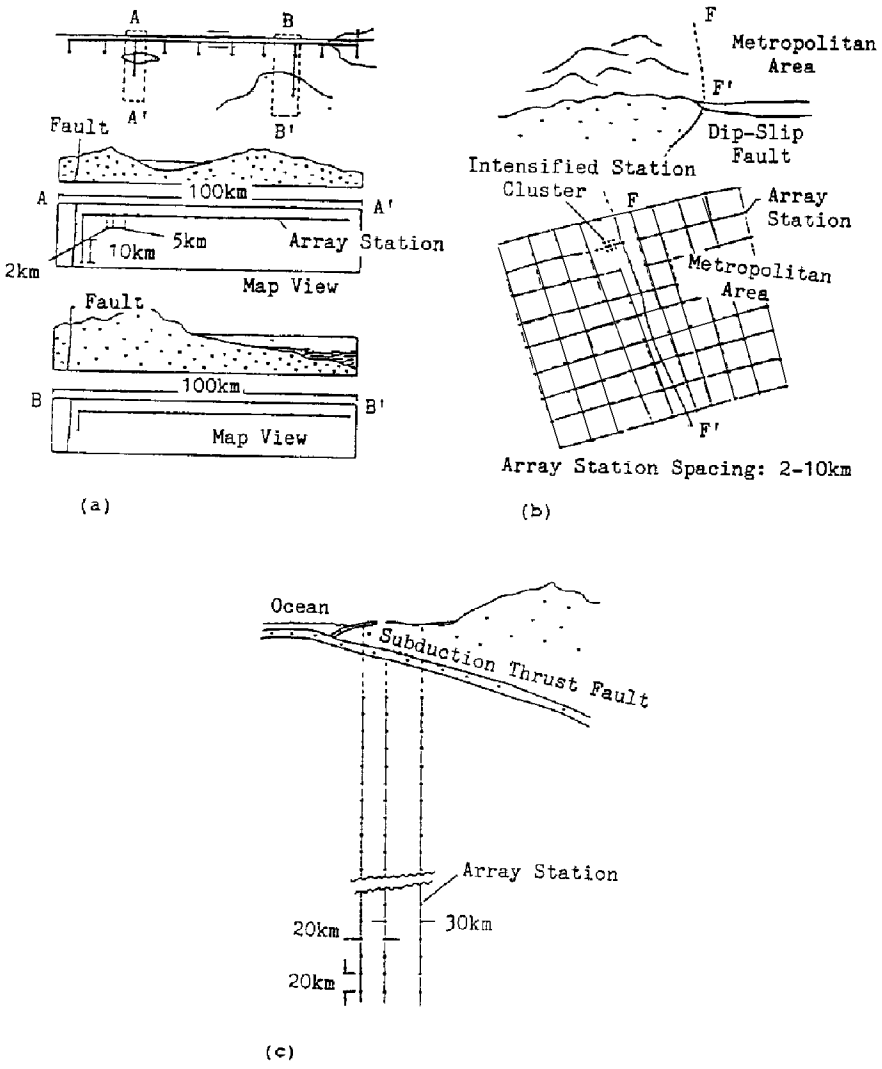

Fig. 1 Array configurations for source mechanism and wave propagation studies recommended at the 1978 International Workshop on Strong-Motion Earthquake Instrument Arrays. (a) Strike-slip; (b) Dip-slip; (c) Subduction thrust fault (after Iwan, 1978)

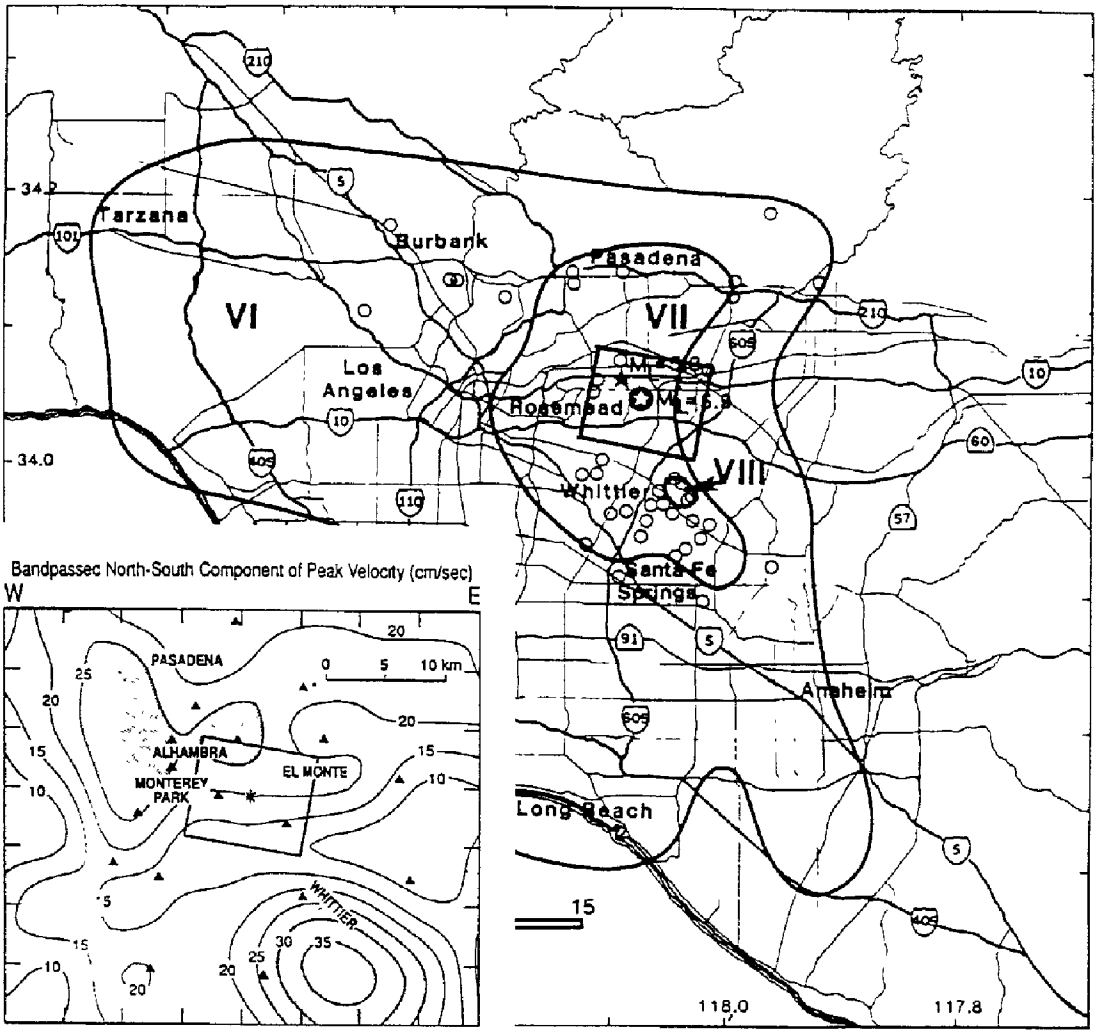

Fig. 2 Regional modified Mercalli intensity iso-seismals in the Los Angeles area for the earthquake of October 1, 1987 Circles = the center of the census traces surveyed; circled star = the main shock epicenter (after Leyendecker *et al.*, 1988). Insert: Predicted peak velocities (cm/s) for model (b) of Figure 3 in the bandpass 0.2 - 3.0 Hz. Values contoured are the peak whole record velocities for the north-south component of motion; triangles = stations used.

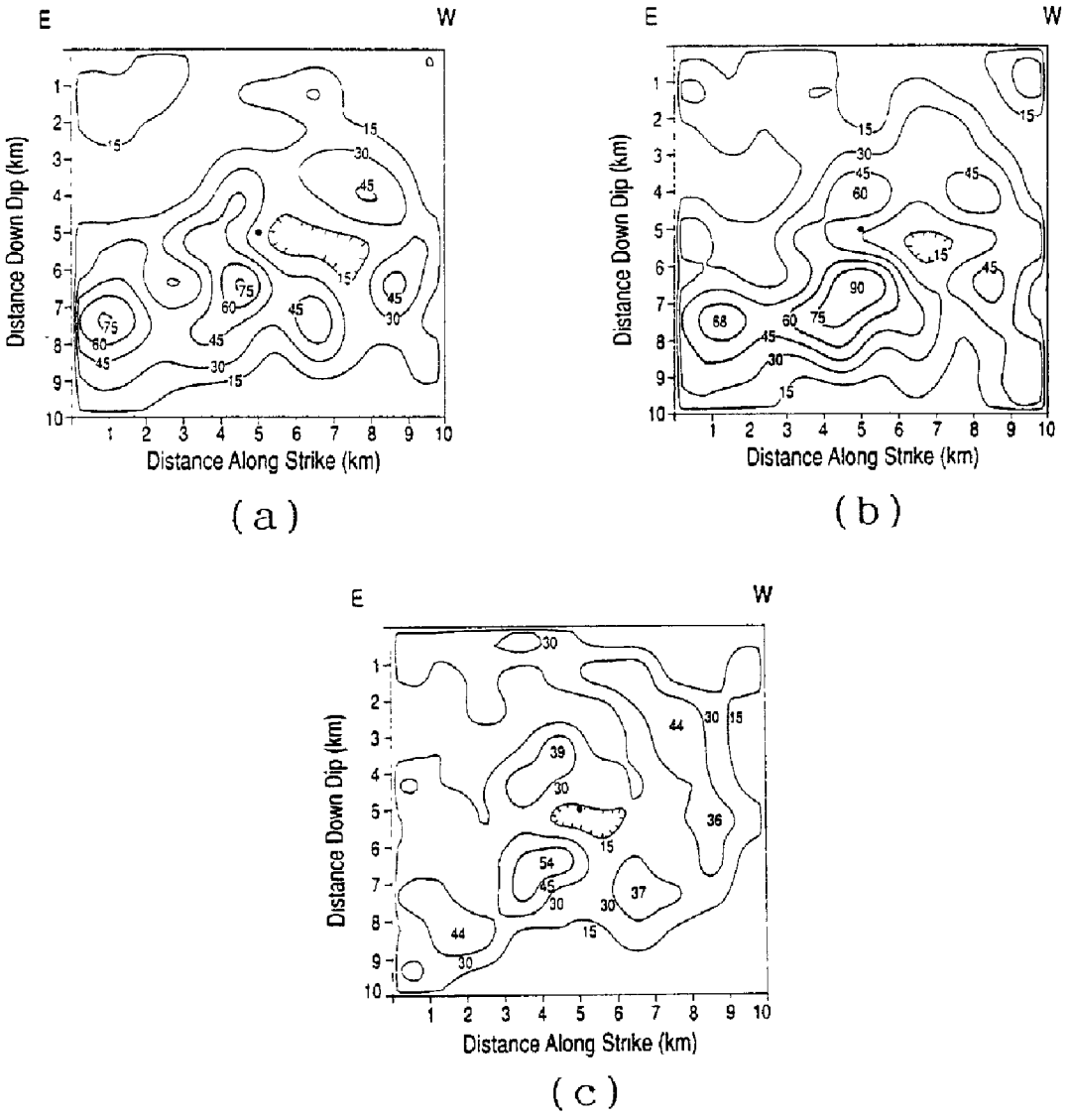

Fig. 3 Contours of slip (in centimeters) for three inversion models. (a) Each subfault ruptures once at a constant rupture velocity of 2.5 km/s. (b) Each subfault is allowed to rupture twice to allow for a more complex source-time function. The rupture velocity is fixed at 2 5 km/s. (c) Each subfault ruptures once, but the rupture velocity is not fixed, and the rupture times for each subfault are free to vary.

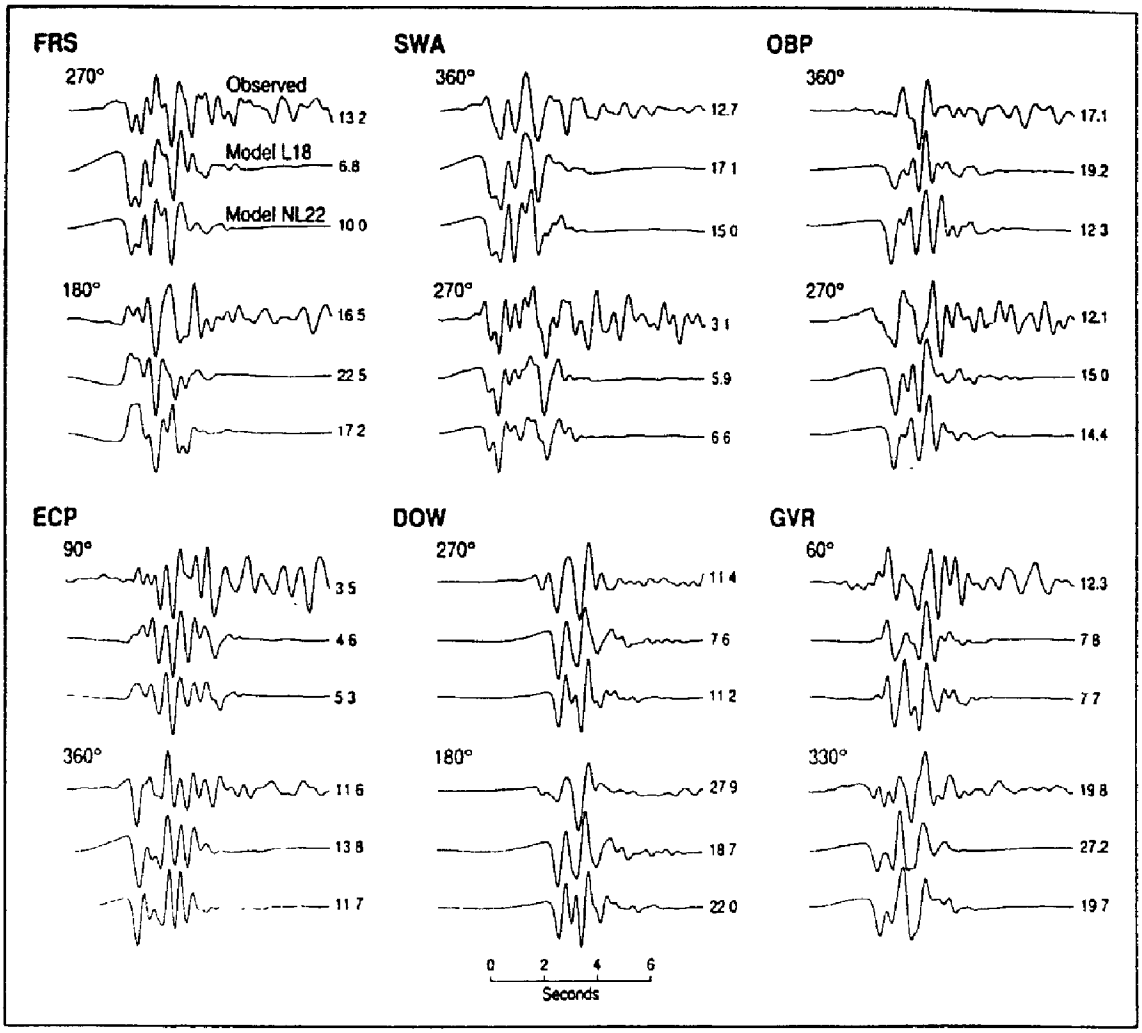

Fig. 4 Comparison of the observed velocity records (first trace) with the synthetic records for model in Fig. 3b (model L18, second trace) and model in Fig. 3c (model NL22, third trace) for six different stations.

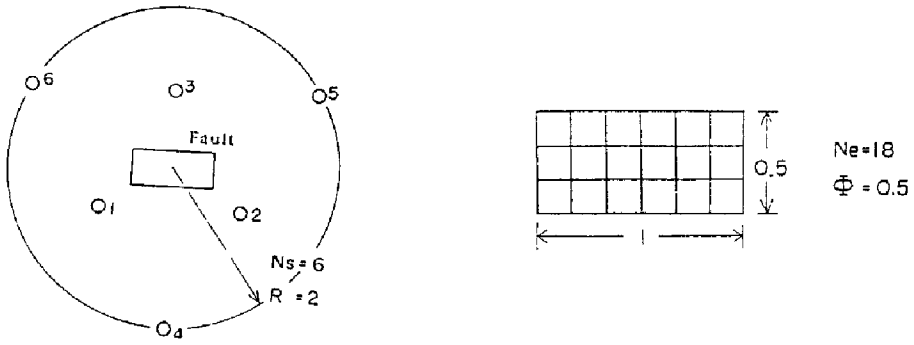

Geometrical arrangement of fault planes and array stations. Two kinds of faults are located at the center of an array: a pure strike-slip fault with a dip angle, $\delta = 90°$ and a pure dip-slip fault with $\delta = 30°$. All the distances are normalized by the fault length.

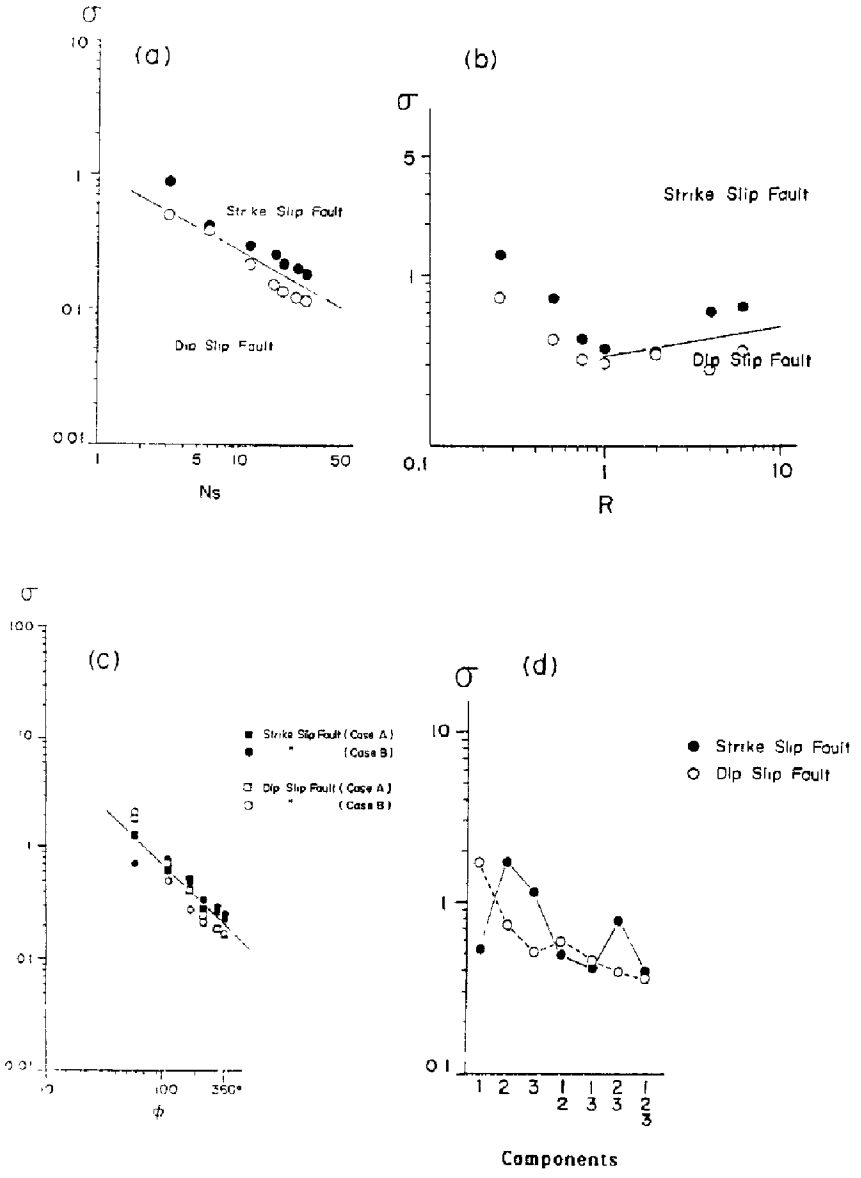

Fig. 6 Relationship between the inversion uncertainty, σ, and array parameters. (a) The number of the stations, N_s. (b) The array radius, R. (c) The azimuthal coverage, ϕ. Case A = rupture propagating towards the array; case B = rupture moving away from the array. (d) The components of the seismograms. 1 = component parallel to the fault strike; 2 = horizontal component perpendicular to the fault strike; 3 = vertical component.

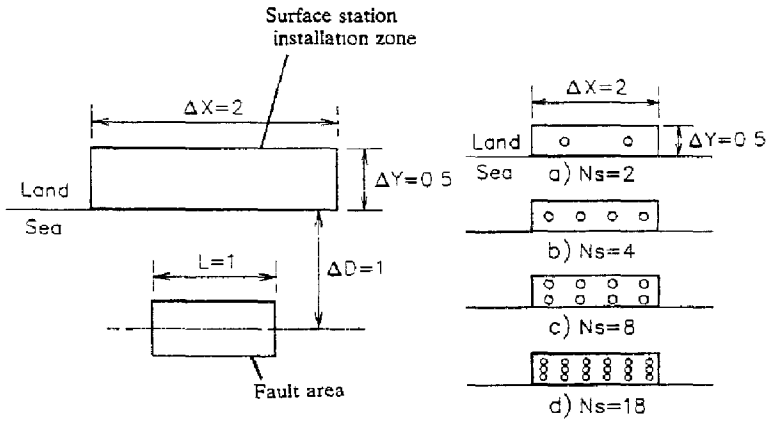

Fig. 7 Geometrical arrangement of fault and array stations for a simulation on an offshore subduction thrust. A pure dip-slip fault with a dip angle, $\delta = 30°$, which is the same as that in Fig. 5, is assumed. The numbers of surface stations and ocean bottom stations, N_s and N_o are varied separately to estimate their influence. The distribution in the surface stations is fixed, based upon the number of surface stations, N_s, and forms a line or a rectangular grid. Several patterns of ocean bottom stations are tested for each pair of N_s and N_o.

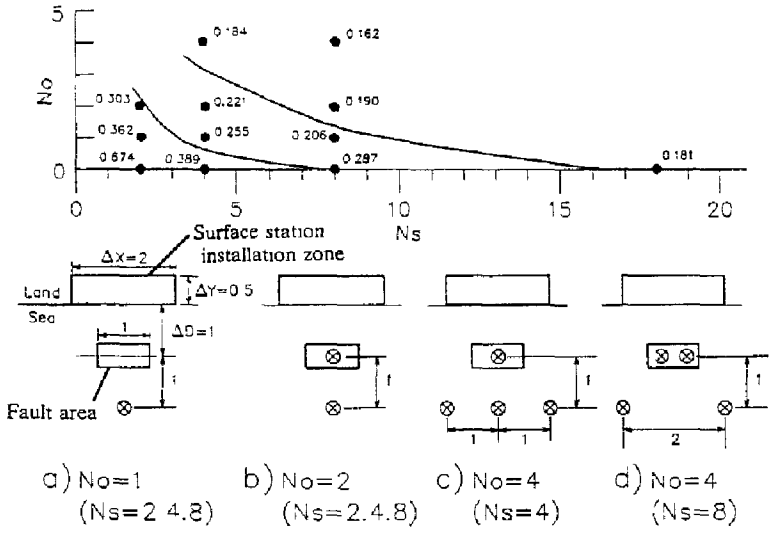

Fig. 8 Relationship among the inversion uncertainty, σ, and the numbers of surface stations and ocean bottom stations, N_s and N_o. The best positions of ocean bottom stations are depicted for each pair of N_s and N_o. We find that, when 1 or 2 ocean bottom seismographs are installed, the locations are not dependent on the number of surface stations, N_s; whereas the locations are changed according to N_s in the case of 4 ocean bottom seismographs.

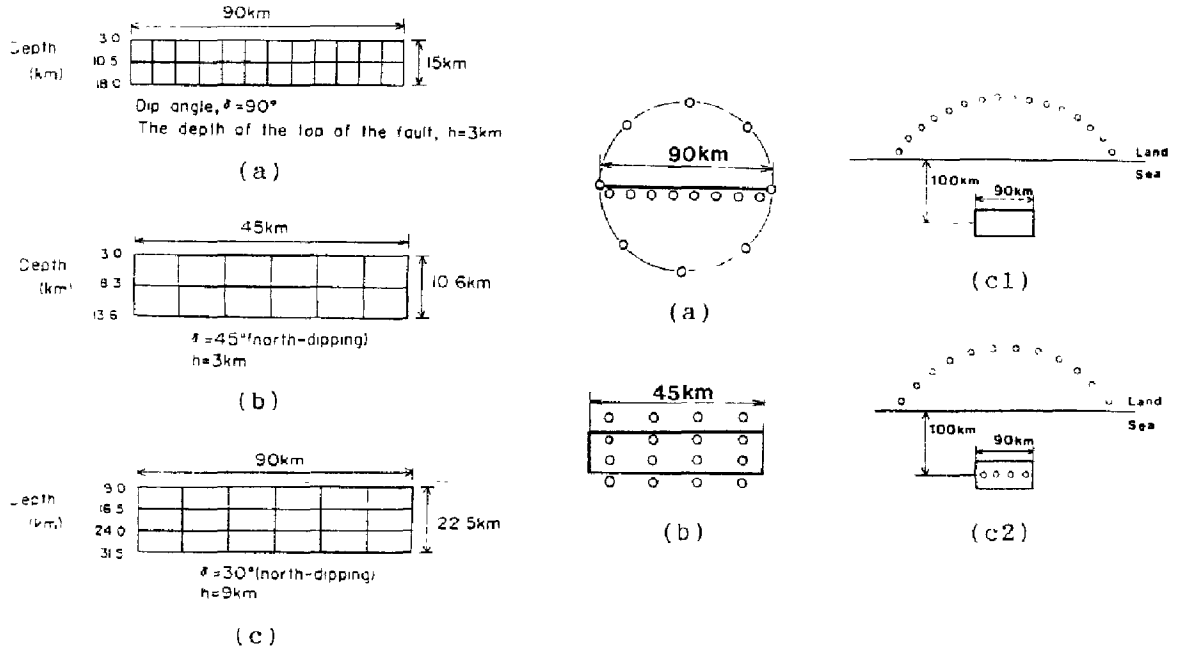

Fig 9 Fault geometries used for investigating effects of array configurations on the source inversion (side views) and the optimum array configuration obtained for each of 3 fault geometries. (a) Strike-slip; (b) Dip-slip; (c) Subduction thrust fault; case c1 = without and c2 = with strong-motion ocean bottom seismograms.

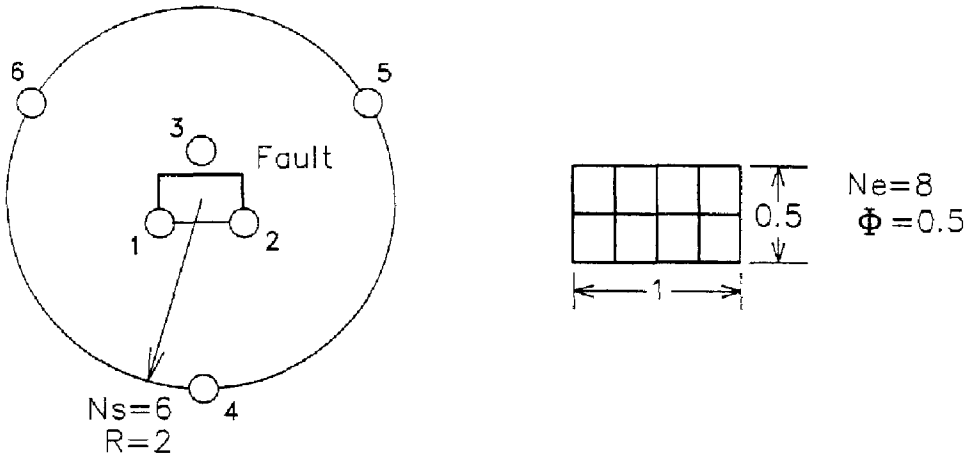

Fig. 10 Geometrical arrangement of fault planes and array stations for studying effects of phase interference and source depth. Three sorts of faults summarized in Table 1 are used. All the distances are normalized by the fault length.

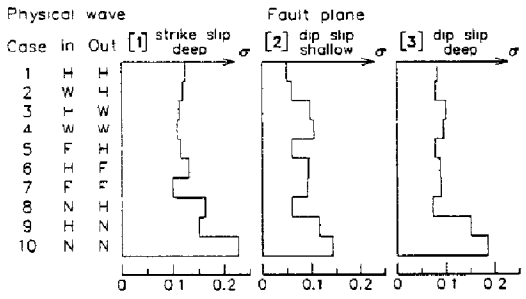

Fig. 11 The accuracy of the source inversion for different fault planes and various physical waves. See Table 1 for the fault planes. In = 3 near-fault stations; Out = 3 other distant stations; H = complete half-space seismograms are used; W = complete wholespace seismograms are used, so surface waves are removed; F and N = only far-field or near-field terms for the wholespace seismograms are used ($W = F + N$).

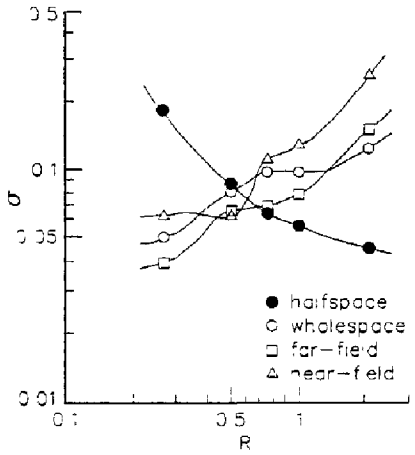

Fig. 12 Relationship between the inversion uncertainty, σ, and the array radius, R, for various physical waves.